Harvesting Nanoscale Thermal Radiation Using Pyroelectric Materials

Jin Fang

Hugo Frederich

Laurent Pilon[1]
e-mail: pilon@seas.ucla.edu

Department of Mechanical and Aerospace Engineering,
Henri Samueli School of Engineering and Applied Science,
University of California, Los Angeles,
Los Angeles, CA 90095-1597

Pyroelectric energy conversion offers a way to convert waste heat directly into electricity. It makes use of the pyroelectric effect to create a flow of charge to or from the surface of a material as a result of heating or cooling. However, an existing pyroelectric energy converter can only operate at low frequencies due to a relatively small convective heat transfer rate between the pyroelectric materials and the working fluid. On the other hand, energy transfer by thermal radiation between two semi-infinite solids is nearly instantaneous and can be enhanced by several orders of magnitude from the conventional Stefan–Boltzmann law as the gap separating them becomes smaller than Wien's displacement wavelength. This paper explores a novel way to harvest waste heat by combining pyroelectric energy conversion and nanoscale thermal radiation. A new device was investigated numerically by accurately modeling nanoscale radiative heat transfer between a pyroelectric element and hot and cold plates. Silica absorbing layers on top of every surface were used to further increase the net radiative heat fluxes. Temperature oscillations with time and performances of the pyroelectric converter were predicted at various frequencies. The device using 60/40 porous poly(vinylidene fluoride–trifluoroethylene) achieved a 0.2% efficiency and a 0.84 mW/cm^2 electrical power output for the cold and hot sources at 273 K and 388 K, respectively. Better performances could be achieved with $0.9Pb(Mg_{1/3}Nb_{2/3})-0.1PbTiO_3$ (0.9PMN-PT), namely, an efficiency of 1.3% and a power output of 6.5 mW/cm^2 between the cold and hot sources at 283 K and 383 K, respectively. These results are compared with alternative technologies, and suggestions are made to further improve the device. [DOI: 10.1115/1.4001634]

Keywords: pyroelectric effect, ferroelectric, direct energy conversion, nanoscale thermal radiation, waste heat harvesting

1 Introduction

Industrial and developing nations are facing the challenge of meeting the rapidly expanding energy needs without further impacting the climate and the environment. Large amounts of energy are lost in the form of waste heat released as a by-product of power, refrigeration, or heat pump cycles, for example. In fact, in 2002 more than 50% of the net primary energy resource consumption in the U.S. was lost mainly in the form of waste heat [1]. Pyroelectric (PE) energy converter offers a novel direct energy conversion technology by directly transforming waste heat into electricity [2–12]. It makes use of the pyroelectric effect to create a flow of charge to or from the surface of a material as a result of successive heating or cooling cycles [13]. However, the operating frequency of the device is usually small (~0.1 Hz) and limited by convective heat transfer between the pyroelectric material and the working fluid subjected to oscillatory laminar flow between a hot and a cold source. This restricts the performance of the device. On the contrary, thermal radiative heat transfer takes place at the speed of light. In addition, the net radiation flux in vacuum between two surfaces at different temperatures can be increased by several orders of magnitude if they are separated by a distance comparable to or smaller than the characteristic wavelength given by Wien's displacement law [14,15]. Thus, nanoscale radiative heat transfer has the potential to increase the operating frequency of pyroelectric energy converters, resulting in a larger power density and efficiency. This paper explores a novel way to combine nanoscale radiative heat transfer and pyroelectric energy conversion in a device harvesting waste heat.

2 Background

2.1 Pyroelectric Materials. Pyroelectric materials feature a spontaneous polarization with strong temperature dependence. The displacement of the atoms from their equilibrium positions gives rise to the spontaneous polarization resulting in the pyroelectric effect. At steady state ($dT/dt=0$), the polarization is constant, and no current is generated. However, a rise in temperature ($dT/dt>0$) reduces the overall polarization through reduction in the dipole moment. The number of bound charges decreases, and the subsequent redistribution of charges results in current flowing in the circuit. If the sample is cooled, the direction of the current is reversed. In an open circuit, the free charges would remain on the electrodes, and a voltage would be established between them. The direction of polarization is usually constant throughout a pyroelectric material, but in some materials this direction can be changed by applying a coercive "poling" electric field [4]. In addition, the relationship between the charge and the open-circuit voltage at a constant temperature features a hysteresis loop [16].

Finally, all ferroelectric materials are pyroelectric, and all pyroelectric materials are piezoelectric. However, the converse is not true. The polarization of ferroelectric materials vanishes beyond the Curie temperature denoted by T_{Curie} when the material undergoes a phase transition from ferroelectric to paraelectric and the spontaneous polarization disappears. This phase transition process results in a large charge release [17]. Differential scanning calorimetry (DSC) measurements for the commercial pyroelectric material 60/40 porous poly(vinylidene fluoride–trifluoroethylene)

[1]Corresponding author.

Contributed by the Heat Transfer Division of ASME for publication in the JOURNAL OF HEAT TRANSFER. Manuscript received October 31, 2009; final manuscript received March 24, 2010; published online June 30, 2010. Assoc. Editor: Robert D. Tzou.

(P(VDF-TrFE)) were reported by Navid et al. [18]. The phase transition from ferroelectric to paraelectric takes place between $T_{p1}=42\,^{\circ}\mathrm{C}$ and $T_{p2}=90\,^{\circ}\mathrm{C}$ with a peak at temperature $T_{\mathrm{Curie}}=65.7\,^{\circ}\mathrm{C}$.

2.2 Direct Pyroelectric Energy Converter. Pyroelectric energy conversion is possible by alternatively placing the pyroelectric material sandwiched between two electrodes in contact with a hot and a cold reservoir. Unfortunately, this process is highly irreversible, and theoretical analysis predicts a low efficiency and a small power density [19–21]. This intrinsic limitation can be attributed to the fact that "the energy required to increase the temperature of the lattice is nearly always much larger than the energy required to destroy part of the polarization thus releasing electric charges" [20].

More recently, Itskovsky [22] noted that the above mentioned analysis [19–21] assumed very small temperature amplitudes of a few milli-Kelvin or Kelvin. Then, the pyroelectric current i is proportional to the time rate of change in temperature $\mathrm{d}T/\mathrm{d}t$, and the pyroelectric effect is linear, i.e., $i=p_c\mathrm{d}T/\mathrm{d}t$, where p_c is the pyroelectric coefficient. However, for energy conversion applications, the amplitude of the temperature oscillation is typically large and the pyroelectric effect is nonlinear. Accounting for these nonlinear effects, Itskovsky [22] studied $LiNbO_3$ featuring $T_{\mathrm{Curie}}=1140\,^{\circ}\mathrm{C}$ [23] and operating with tens of kelvin amplitude within the phase transition region. The author theoretically established that "the instantaneous energy conversion efficiency for ferroelectrics with parameters similar to those of $LiNbO_3$ type can reach over 20% in the relaxation process on cooling."

Moreover, the performance of pyroelectric energy converter can be significantly improved by using heat regeneration and multistages along with the Olsen cycle [2–5]. To date, only five prototypes of pyroelectric converters have been built. First, Olsen and co-workers [2,4,5] experimentally demonstrated 1 mW and 40 mW devices with an efficiency around 0.4% [4] but 16 times greater than the maximum efficiency predicted by van der Ziel [21]. They used lead zirconate titanate (PZT) as pyroelectric materials and silicone oil as the working fluid while they operated between 145 °C and 178 °C [4]. Later, Olsen et al. [3] assembled the only multistage device built to date using different grades of lead zirconate stannate titanate (PZST), in which Ti^{4+} was substituted by Sn^{4+} for a maximum output of 33 W/l of pyroelectric materials at 0.26 Hz and featuring a maximum thermodynamic efficiency of 1.05% at 0.14 Hz or 12% of the Carnot efficiency. Moreover, due to the cost of PZT ($10,000/W), Olsen et al. [6] proposed to use inexpensive single stage 73/27 P(VDF-TrFE) films 30–70 μm thick sandwiched between electrodes and rolled in a spiral stack placed into a cylindrical chamber containing silicone oil. The energy density between 20 °C and 90 °C achieved 30 mJ cm^3/cycle. Recently, Nguyen et al. [12] built and tested a pyroelectric converter using 60/40 P(VDF-TrFE) and achieved a maximum energy density of 130 J/l at a 0.061 Hz frequency with a temperature oscillating between 69.3 and 87.6 °C. Furthermore, a maximum power density of 10.7 W/l was obtained at 0.12 Hz between 70.5 °C and 85.3 °C. In all these prototypes, the pumping was performed by a step motor with a piston amplitude of 2–10 cm. Ceramic stacks were used to reduce axial heat conduction and ensure laminar flow of the working fluid over the pyroelectric elements as turbulence would result in the mixing of the cold and hot fluids and would disrupt the oscillating temperature gradient. Theoretically, pyroelectric conversion based on heat regeneration and the Olsen cycle can reach the Carnot efficiency between a hot and a cold thermal reservoir [3,24]. Limitations in reaching the Carnot efficiency include (i) hysteretic and resistive losses, (ii) heat losses to the surrounding, and (iii) sensible (thermal) energy.

Furthermore, the electrocaloric effect corresponds to a change in material temperature upon application or withdrawal of an electric field under adiabatic condition. Consequently, a material having a very large electrocaloric activity also features a large pyroelectric energy harvesting capability [25]. The ratio of pyroelectric conversion efficiency to the Carnot efficiency increases as the temperature difference decreases. For a very small temperature difference, it is possible to harvest energy with Carnot efficiency [25]. In particular, a giant electrocaloric effect in a $0.9Pb(Mg_{1/3}Nb_{2/3})-0.1PbTiO_3$ composite thin film, also called 0.9PMN-PT, around 348 K was reported upon the application or withdrawal of an electric field of 895 kV/cm [26]. More recently, Sebald et al. [25] estimated an associated energy density of 432 J/l for pyroelectric conversion between 338 K and 348 K by using 0.9PMN-PT thin films about 260 nm in thickness.

2.3 Nanoscale Radiation. Based on the theory of electrical fluctuation and thermal radiation [27], it was shown that energy transfer by thermal radiation between two semi-infinite solids can be enhanced by several orders of magnitude if the vacuum gap size is smaller than the radiation peak wavelength given by Wien's displacement law ($\lambda_{\max}T=2898$ μm K) [14,15]. This can be attributed to (i) propagating wave interferences and (ii) tunneling of the evanescent waves across the gap [15]. Wave interferences take place in the vacuum gap due to multiple reflections at the gap/solid interfaces. Radiation tunneling relies on evanescent surface waves that decay exponentially with distance as it travels through the gap. These surface waves appear when total reflection occurs on the interface between two materials. They are due to coupling between the material resonant polarization oscillation and the electromagnetic field, also called polaritons. In the case of metals, these surface waves are supported by charged carriers and are called surface plasmon polaritons. In the case of dielectrics materials, the surface waves are supported by phonons and are called surface phonon polaritons. Surface phonon polaritons are excited by infrared radiation, while surface plasmon polaritons are excited in the visible or near-UV domain [28]. If the gap is small compared with $\lambda_{\max}$, the time-averaged Poynting vector associated with the evanescent wave incident on the surface is different from zero and energy tunnels across the gap. Nanoscale radiation has found applications in thermophotovoltaic devices [29,30] and in scanning thermal microscopy [31], for example.

Most studies on nanoscale radiative transfer have been theoretical in nature, and only a few experimental studies have been reported. One of the first experimental studies was performed by Hargreaves [32], who studied the effect of gap size on the net radiation heat transfer between two parallel glass plates coated with 0.1 μm thick chromium films at temperatures of $T_1=323$ K and $T_2=306$ K, respectively. The plate separation and parallelism were adjusted by means of piezoelectric ceramic pillars. The apparatus was placed in a vacuum chamber evacuated to 10^{-5} torr. The author observed that the net heat transfer rate between the plates deviated from the classical surface radiation theory for a distance less than 3 μm. He attributed this to the "proximity effect," but no quantitative comparison with theory was performed. Polder and Van Hove [15] theoretically found a qualitative agreement with experimental results by Hargreaves [32] but not in terms of absolute magnitudes. Similarly, Domoto et al. [33] studied radiative heat transfer between two parallel copper plates at a cryogenic temperature, but discrepancies between experimental and theoretical predictions were very large and were attributed to poor parallelism between the plates and to poor knowledge of optical properties. DiMatteo et al. [29] measured the photocurrent in an actively cooled thermophotovoltaic cell placed close to a heated surface. The authors found that their measurements were qualitatively consistent with theoretical predictions. However, Kittel et al. [34] found the contrary by measuring the power absorbed or emitted by the tip of a thermal profiler and a planar surface under high vacuum conditions. At distances below 10 nm, their experimental results deviated significantly from the predictions from fluctuating electrodynamics. They attributed this to scale effects in which the macroscopic description of dielectric properties fails below a certain size. Other

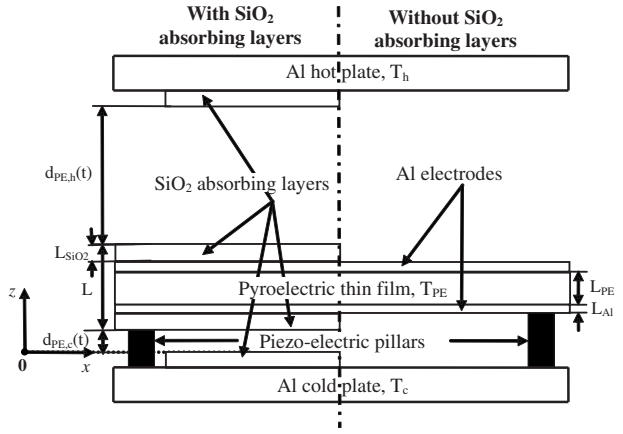

Fig. 1 Schematic of the PE plate as it oscillates between the hot and cold plates, with or without SiO_2 absorbing layers (not to scale)

possible reasons for discrepancies included poor parallelism between the plates, and the assumption of a semi-infinite plate might not be satisfied experimentally. Similarly, Pan [35] and Pan et al. [36] questioned the approach used in other theoretical studies computing the heat transfer between metal and dielectric plates [37,38]. More recently, Hu et al. [39] showed that the temperature dependence for the heat flux between two parallel glass surfaces at temperatures of 23°C and 50°C placed in vacuum and separated by a gap of 1.6 μm agreed with the theory. The authors used small polystyrene particles as spacers to maintain a micron-sized gap. Narayanaswamy et al. [40] measured radiative transfer between a silica sphere and a flat silica surface. The presence of strong near-field effects enhanced radiative heat transfer over the predictions of the Planck blackbody radiation theory [40,41]. Shen et al. [42] measured radiation heat transfer between a glass microsphere hotter by 16.5 K than flat surfaces at ambient temperature and made of glass, doped silicon, and Au down to 30 nm separation. The net energy transfer was the largest when the two surfaces were made of glass when it was three orders of magnitude larger than that of the blackbody radiation limit.

In addition, the effect of metallic or dielectric thin film coatings on the near-field radiative heat transfer between two plane surfaces is important from a fundamental as well as from an application point of view. Recent studies showed that the surface plasmon polariton excited in a metallic coating a few nanometers thick deposited on a metallic or dielectric substrate can significantly increase the radiative heat flux [43,44]. On the other hand, surface phonon polaritons are easier to excite thermally at low temperatures ($\sim$300 K) than surface plasmon polaritons since the resonant frequency of surface phonon polaritons is in the infrared region [45,46]. For example, the total radiative flux between a SiC slab set at 0 K and a metallic substrate [46] or a dielectric substrate [45] set at 300 K was shown to increase by coating the latter with a few nanometer thick SiC film. In addition, when the coating thickness exceeds 1 μm, Fu and Tan [46] showed that the contribution to the near-field radiative flux from the substrate was negligible and the heat flux was entirely contributed by the coating.

3 Analysis

3.1 Device Principle. Figure 1 illustrates a conceptual device combining nanoscale radiation and pyroelectric energy conversion consisting of a hot and cold plane-parallel plates and an oscillating PE plate. The PE plate is composed of a pyroelectric material film of thickness L_{PE} sandwiched between aluminum electrodes of thickness L_{Al} used to collect the electric charges and to apply an electric field. The hot and cold plates are made of aluminum. SiO_2 thin films of thickness L_{SiO_2} can be coated on both sides of the PE plate and on the hot and cold surfaces as absorbing layers, which emit and absorb nanoscale radiation to enhance radiative heat transfer. The total thickness of the PE plate is denoted by L_t. The hot plate is at temperature T_h, and the cold plate is at temperature T_c. The distances between the hot/cold plates and the PE plate are denoted by $d_{PE,h}$ and $d_{PE,c}$, respectively. The PE plate is mounted on piezoelectric pillars, which make it oscillate between the hot and cold plates. The entire device is operated under vacuum to minimize both friction on the oscillating PE plate and heat losses to the surroundings. In addition, the presence of air in the gap would hinder the temperature oscillations in the PE plate caused by nanoscale thermal radiation as heat conduction may dominate.

3.2 Assumptions. To make the problem mathematically trackable, the following assumptions have been made:

1. Hot and cold plates are assumed to be semi-infinite; i.e., end effects are neglected.
2. The absorbing SiO_2 layers and the electrodes are considered to be opaque and can be treated as semi-infinite. Indeed, a dielectric material such as SiO_2 exhibits a large absorption index at the peak wavelength λ_{max} around 8–10 μm at the temperatures of interest (300–400 K).
3. The absorbing layers deposited on the hot and cold plates are assumed to be at the same temperatures as the plates, namely, T_h and T_c, respectively.
4. Complex dielectric constants of metals and dielectric materials considered are modeled by the Drude and Lorentz models, respectively.
5. All properties are assumed to be independent of temperature.
6. The temperature is assumed to be uniform across the PE plate.
7. The location of the PE plate over time is assumed to be a step function. This is justified by the fact that the displacement of the PE plate is much faster than the temperature changes in the PE plate.
8. The pyroelectric material, which is also ferroelectric exhibits a very large charge redistribution across the phase transition from ferroelectric to paraelectric. A large part of the energy density denoted by N_D produced at every cycle is contributed from this phase transition. Thus, N_D is assumed to be constant and equal to the energy density generated by operating the Olsen cycle across the phase transition, as long as the operating temperature span is wider than the phase transition interval between $T_{p,1}$ and $T_{p,2}$.

3.3 Governing Equation. For an elementary element of the composite PE plate with a unit surface area and thickness L_t, the energy conservation equation can be written as

$$(\rho c_p)_{\text{eff}} L_t \frac{dT_{\text{PE}}}{dt} = q''_{h\to\text{PE}}(T_h, T_{\text{PE}}, d_{\text{PE},h}) - q''_{\text{PE}\to c}(T_{\text{PE}}, T_c, d_{\text{PE},c}) \tag{1}$$

where $(\rho c_p)_{\text{eff}}$ is the effective volumetric heat capacity of the composite PE plate. The heat flux $q''_{h\to\text{PE}}$ and $q''_{\text{PE}\to c}$ are the net radiative heat fluxes from the hot plate to the PE plate and from the PE plate to the cold plate, respectively. The generic radiative heat flux $q''_{1\to 2}(T_1, T_2, d)$ appearing in Eq. (1) accounts for the far-field (propagative) and the near-field (evanescent) contributions to the total radiative heat flux between two semi-infinite media 1 and 2 separated by a distance d and at temperatures T_1 and T_2, respectively. It can be estimated from the fluctuating electrodynamic theory [27] and is written in the general form as [28,47]

$$q''_{1\to 2}(T_1,T_2,d)=\int_0^\infty [I^0_{b\omega}(T_1)-I^0_{b\omega}(T_2)]\times\Phi_{12}(\omega,d)\mathrm{d}\omega \quad (2)$$

where $I^0_{b\omega}(T)$ is the spectral blackbody radiation intensity at frequency ω and temperature T, given by Planck's law as [48]

$$I^0_{b\omega}(T)=\frac{\omega^2}{4\pi^3c^2}\frac{\hbar\omega}{(e^{\hbar\omega/k_BT}-1)} \quad (3)$$

where $\hbar$ is the reduced Planck constant, c is the speed of light in vacuum, and k_B is the Boltzmann constant. The function $\Phi_{12}(\omega,d)$ corresponds to the spectral efficiency in radiative heat transfer between media 1 and 2 separated by a distance d and is expressed as [49]

$$\Phi_{12}(\omega,d)=\sum_{j=\mathrm{s,p}}\left(\int_{q=0}^{\omega/c}\frac{qc^2}{\omega^2}\frac{(1-|r^j_{31}|^2)(1-|r^j_{32}|^2)}{|1-r^j_{31}r^j_{32}e^{2ipd}|^2}\mathrm{d}q\right)+\sum_{j=\mathrm{s,p}}\left(\int_{q=\omega/c}^{\infty}\frac{qc^2}{\omega^2}\frac{4e^{-2|p|d}\,\mathrm{Im}(r^j_{31})\mathrm{Im}(r^j_{32})}{|1-r^j_{31}r^j_{32}e^{-2|p|d}|^2}\mathrm{d}q\right) \quad (4)$$

where p and q are the z- and x-components of the wavevector in the vacuum gap, respectively. They are related by $p=\sqrt{(\omega/c)^2-q^2}$, where ω/c is the amplitude of the wavevector. Summation is made to account for both s- and p-polarizations. The first term on the right-hand side of Eq. (4) corresponds to the far-field radiation contribution. Integration over q from 0 to ω/c accounts for all propagative waves and results in the Stefan–Boltzmann law. The second term represents the contribution of the near-field radiation to the total radiative heat flux. Integration over q from ω/c to infinity stands for the evanescent waves or the tunneling heat flux. It is evident that the amplitude of evanescent waves decreases exponentially as the distance d between the plates increases. The near-field term is negligible compared with the first term for large distance d [28]. Note that Eq. (4) includes integration over the azimuthal angle and accounts for interferences and polaritons coupling between the two media.

The Fresnel coefficients for s- and p-polarized electromagnetic waves incident from medium 3 (vacuum) on the interface with medium 1 are denoted by r_{31} and expressed, for s- and p-polarizations, as [50]

$$r^s_{31}=\frac{p-s_1}{p+s_1}\quad\text{and}\quad r^p_{31}=\frac{\varepsilon_{r1}p-s_1}{\varepsilon_{r1}p+s_1} \quad (5)$$

where ε_{r1} is the complex dielectric constant of medium 1, while $s_1=\sqrt{\varepsilon_{r1}\omega^2/c^2-q^2}$ is the z-component of the wavevector in medium 1. Fresnel coefficients r^s_{32} and r^p_{32} between media 2 and 3 are obtained in a similar manner. Note that all these parameters depend on ω.

Finally, the net radiative heat fluxes $q''_{h\to\mathrm{PE}}$ and $q''_{\mathrm{PE}\to c}$ were computed from Eqs. (2)–(5) for distance d and temperature $T_{\mathrm{PE}}(t)$. Then, Eq. (1) was solved for the PE plate temperature $T_{\mathrm{PE}}(t)$ as a function of time.

3.4 Initial Conditions. The initial PE plate temperature at time $t=0$ was set to be $T_{\mathrm{PE}}(t=0)=(T_c+T_h)/2$. The PE plate oscillated at frequency f between hot and cold plates separated by a gap of 100 μm and maintained at constant temperatures T_h and T_c, respectively. The distances $d_{\mathrm{PE},h}$ and $d_{\mathrm{PE},c}$ were step functions of time and oscillated at a frequency f and were such that $L_t+d_{\mathrm{PE},h}(t)+d_{\mathrm{PE},c}(t)=100$ μm. Their minimum value was arbitrarily set at 100 nm, which has been achieved experimentally [42] while ensuring that the near-field radiative heat transfer dominates radiation transfer successively between the PE plate and the cold and hot plates. Note also that the PE plate oscillation can be achieved using conventional piezoelectric actuators [51]. Initially, the PE plate was positioned so that $d_{\mathrm{PE},c}(t=0)=100$ nm.

3.5 Constitutive Relations. Constitutive relationships for the dielectric constant ε_{ri} of each medium i are necessary in order to compute the Fresnel coefficients as a function of angular frequency ω given by Eq. (5). The Drude model is widely accepted to predict the complex dielectric constant of metals and is expressed as [50]

$$\varepsilon_r(\omega)=1-\frac{\omega_p^2}{\omega^2-i\gamma\omega} \quad (6)$$

where ω_p is the plasma frequency and γ is the relaxation frequency. On the other hand, the dielectric constant for dielectric materials is given by the Lorentz model [50],

$$\varepsilon_r(\omega)=1-\frac{\omega_p^2}{\omega_0^2-\omega^2-i\gamma\omega} \quad (7)$$

where ω_0 is the oscillator frequency. Multiple oscillators can be accounted for by adding terms similar to the second term on the right-hand side of Eqs. (6) and (7) with different oscillator, plasma, and relaxation frequencies. Here, the Drude model was used for aluminum with parameters $\omega_p=2.4\times10^{16}$ rad/s and $\gamma=1.25\times10^{14}$ rad/s [43]. The Lorentz model was used for SiO_2 with parameters $\omega_p=1.696\times10^{14}$ rad/s, $\omega_0=2.0\times10^{14}$ rad/s, and $\gamma=5.65\times10^{12}$ rad/s [50]. They were shown to accurately predict the optical properties of aluminum and SiO_2 in the frequency range of interest [43,50].

Simulations were performed for a single film of pyroelectric material of thickness $L_{\mathrm{PE}}=25$ μm sandwiched between two aluminum electrodes (Al) of thickness $L_{\mathrm{Al}}=1$ μm. Unless otherwise noticed, the Al electrodes were coated with a SiO_2 absorbing coating of thickness $L_{\mathrm{SiO_2}}=1.5$ μm to enhance the radiative heat flux, as previously discussed. Thus, the total thickness L_t of the composite PE plate was 30 or 27 μm with or without SiO_2 absorbing coating, respectively. The effective volumetric heat capacity $(\rho c_p)_{\mathrm{eff}}$ in the presence of absorbing layers was taken as

$$(\rho c_p)_{\mathrm{eff}}=\frac{1}{L_t}[(\rho c_p)_{\mathrm{PE}}L_{\mathrm{PE}}+2(\rho c_p)_{\mathrm{Al}}L_{\mathrm{Al}}+2(\rho c_p)_{\mathrm{SiO_2}}L_{\mathrm{SiO_2}}] \quad (8)$$

where $(\rho c_p)_i$ is the volumetric heat capacity of medium i, be it a pyroelectric element (PE), aluminum (Al), or silicon dioxide (SiO_2). For the PE plate made of 60/40 P(VDF-TrFE) with SiO_2 absorbing layers, $\rho_{\mathrm{PE}}=1930$ kg/m^3, $c_{p,\mathrm{PE}}=1200$ J/kg K [17], $(\rho c_p)_{\mathrm{eff}}$ was found equal to 2.31×10^6 J/m^3 K. In the absence of SiO_2 absorbing layers, $(\rho c_p)_{\mathrm{eff}}$ was equal to 2.33×10^6 J/m^3 K.

3.6 Method of Solution. The PE plate temperature $T_{\mathrm{PE}}(t)$ was determined by solving Eq. (1). The latter was solved numerically for $T_{\mathrm{PE}}(t)$ using a finite-difference method based on the forward-difference approximation for the time derivative. This yields the following explicit expression for T_{PE} at time $t+\Delta t$ knowing its value at time t,

$$T_{\mathrm{PE}}(t+\Delta t)=T_{\mathrm{PE}}(t)+\frac{q''_{h\to\mathrm{PE}}(T_h,T_{\mathrm{PE}}(t),d_{\mathrm{PE},h}(t))-q''_{\mathrm{PE}\to c}(T_{\mathrm{PE}}(t),T_c,d_{\mathrm{PE},c}(t))}{(\rho c_p)_{\mathrm{eff}}L_t}\Delta t \quad (9)$$

where Δt is the time step. The net radiation fluxes $q''_{h\to\mathrm{PE}}$ and $q''_{\mathrm{PE}\to c}$ were computed numerically at every time step according to Eqs. (2)–(5) where the integrals over frequency ω and over the x-component of the wavevector q were performed using the Simpson 3/8 rule. Integration over ω from 0 to infinity was performed up to $\omega=N_\omega k_BT_1/\hbar$, where k_B is the Boltzmann constant. Integration over q from ω/c to infinity was performed up to $q=N_q\omega/c$. Here, N_ω and N_q are the numbers of frequencies and wavevectors considered. Numerical convergence for $q''_{h\to\mathrm{PE}}$ and $q''_{\mathrm{PE}\to c}$ was es-

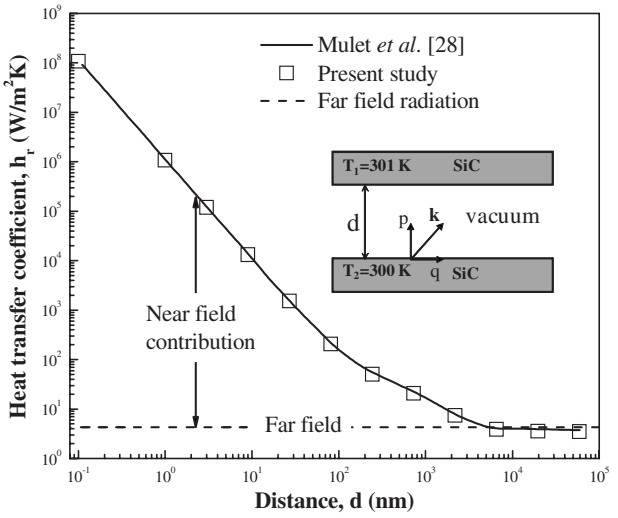

Fig. 2 Comparison between results obtained in the present study with results reported by Mulet et al. [28] for the heat transfer coefficient between two semi-infinite bodies of SiC at 300 K and 301 K as a function of distance d ($\lambda_{max} \simeq 10^4$ nm)

tablished by reducing $\Delta\omega$ and Δq and increasing N_ω and N_q by a factor of 1.3 until the numerical results did not vary by less than 0.1% for the heat fluxes $q''_{h\to PE}$ and $q''_{PE\to c}$. Numerical convergence for $T_{PE}(t)$ was established by reducing Δt by a factor of 1.6 until the results did not vary by less than 1% for all time steps.

When the gap is large ($\sim$100 μm), the SiO_2 thin films cannot be treated as opaque or semi-infinite. However, the net heat flux through the smaller gap is always much larger than that through the larger gap on the other side of the PE plate. In other words, heat transferred through the larger gap does not contribute significantly to the net total heat flux received by the PE plate and therefore has no effect on its temperature oscillation.

3.7 Validation. Validation of the computer program developed in this study was performed for identical plane-parallel semi-infinite solids separated by a vacuum gap of thickness d. The results were compared with those reported in the literature for both metallic and dielectric materials.

First, the radiation heat flux between two silver plates at temperatures 0 K and 273 K was computed using the Drude model with parameters $\omega_p = 1.4\times10^{16}$ rad/s and $\gamma = 2.5\times10^{13}$ rad/s [43]. The numerical results from the code developed in this study fell within 0.1% of those reported by Volokitin and Persson [47] for distances between 1 nm and 1 μm.

A radiative heat flux between dielectric materials at 300 K can be even larger than that for silver, as shown by Mulet et al. [28]. This is due to their dielectric constant, which enables a high coupling between the surface waves in the infrared part of the spectrum. Numerical calculations were performed for parallel semi-infinite plates of SiC at temperatures of 300 K and 301 K, respectively. The radiative heat transfer coefficient h_r was defined as $h_r(d) = \lim_{T_1\to T_2}[q''_{1\to2}(T_1,T_2,d)/(T_1-T_2)]$. The parameters for SiC used in the Lorentz model were $\omega_p = 2.72\times10^{14}$ rad/s, $\omega_0 = 1.49\times10^{14}$ rad/s, and $\gamma = 8.97\times10^{12}$ rad/s [52]. The radiative heat transfer coefficient at 300 K calculated from far-field radiation by the Stephan–Boltzmann law was also given for comparison purposes. The far-field radiation heat flux was expressed as $q''_{1\to2} = \sigma(T_1^4 - T_2^4)/(2/\alpha_1 - 1)$, where $\sigma = 5.67\times10^{-8}$ W/m^2 K^4 is the Stefan–Boltzmann constant and $\alpha_1 = \alpha_2$ is the total hemispherical emissivity of SiC at 300 K such that $\alpha_1 = 0.83$ [48]. Figure 2 shows the radiative heat transfer coefficient h_r between two semi-infinite bodies of SiC as a function of distance d. It is evident that the numerical results obtained agree well with those reported by Mulet et al. [28], and the heat flux is enhanced by several orders of magnitude compared with the far-field radiative heat flux when the gap size becomes smaller than $\lambda_{max} = 10^4$ nm.

3.8 Thermodynamic Efficiency of the Device. In order to assess the performance of the proposed pyroelectric device, the average thermodynamic efficiency over a cycle is defined as

$$\eta = \frac{\dot{W}_e - \dot{W}_p}{\dot{Q}_{in}} \tag{10}$$

where $\dot{W}_e$ is the electric power generated by the PE plate and $\dot{W}_p$ is the power provided by the piezoactuators, both per unit surface area of the PE plate and expressed in W/m^2. The heat flux (in W/m^2) provided by the hot plate to the PE plate over one cycle of period τ is denoted by $\dot{Q}_{in}$ and expressed as

$$\dot{Q}_{in} = \frac{1}{\tau}\int_0^\tau q''_{h\to PE}(T_h, T_{PE}, d_{PE,h}(t))\,d\tau \tag{11}$$

where $\tau = 1/f$ is the oscillation period.

In order to estimate the power $\dot{W}_p$, the pressure balance on the PE plate was performed. The main forces affecting the motion of the PE plate are (i) the gravitational force, (ii) the Casimir force, (iii) the van der Waals force, and (iv) the radiation pressure force.

Assuming that the oscillation is vertical, the gravitational force acting on the PE plate has to be overcome by the piezoelectric pillars. The gravitational force per unit surface area is given by $P_g = \rho_{eff} L_t g$, where g is the gravitational acceleration ($g = 9.81$ m/s^2). Given the PE plate thickness $L_t = 30$ μm and its effective density of $\rho_{eff} = 2.10$ g/cm^3, the gravitational pressure P_g was estimated to be about 0.6 Pa.

The Casimir force is an attractive force between surfaces caused by the quantum fluctuations in the zero point electromagnetic field [53]. In the present study, when the parallel plates get close to each other, the Casimir force, negligible at macroscale, becomes important. The attractive Casimir force per unit surface area for semi-infinite parallel metallic plates is expressed as $P_c = -\pi^2\hbar c/240d^4$ [51]. Thus, the Casimir force acting between two metallic plane-parallel plates distant by $d = 100$ nm amounts to 13 Pa. When the two plates are made of dielectric materials (e.g., SiO_2 and SiC), the Casimir force is typically smaller by one order of magnitude [54]. Moreover, if the two plates are not perfectly parallel and the closest distance between them is the same as the distance between parallel plates, the Casimir force will be even lower [55].

The van der Waals force is often responsible for the adhesion in microscale devices. For two parallel flat plates in vacuum, the van der Waals pressure is expressed as $P_v = -H/12\pi d^2$, where H is the Hamaker constant and d is the distance separating the two surfaces [56]. The Hamaker constant of most condensed phases with an interaction across the vacuum is found to lie in the range from 0.4 to 4×10^{-19} J [56]. In the present study, the minimum distance between the PE plate and the hot/cold plates was assumed to be 100 nm. Then, the adhesive pressure due to the van der Waals force was less than 1×10^{-6} Pa.

Moreover, the radiation pressure on the plates is given by $P_{rad} = \dot{Q}_{in}/c$ [57]. The magnitude of the average heat transfer rate $\dot{Q}_{in}$ is about 1 W/cm^2, corresponding to a radiation pressure around 10^{-5} Pa.

Consequently, both P_{rad} and P_v are negligible compared with P_g and P_c, and the time-averaged oscillation power $\dot{W}_p$ per unit surface area needed from the piezoelectric pillars can be expressed as

$$\dot{W}_p = \frac{2}{\tau}\int_{z_1}^{z_2} (P_g/2 + P_c)\mathrm{d}z \tag{12}$$

where τ is the oscillation period, and $z_1 = d_{\mathrm{PE},c}(t=0) = 0.1$ μm and $z_2 = d_{\mathrm{PE},c}(t=\tau/2) = 69.9$ μm are the minimum and maximum gaps between the PE plate and the cold plate. Note that the gravitational pressure P_g needs to be overcome only in the ascending motion of the PE plate.

The electrical energy density N_D is defined as the electrical energy generated per cycle and per unit volume of the pyroelectric material and can be determined experimentally by operating the Olsen cycle across the phase transition interval between temperatures T_{p1} and T_{p2} [6,10,17]. Then, according to Assumption 8, the electrical power density generated by the device at a given frequency can be estimated. If the thickness of the PE thin film is denoted by L_{PE}, the electrical power generated at frequency f per unit surface area of the PE plate is given by

$$\dot{W}_e = fL_{\mathrm{PE}}N_D \tag{13}$$

3.9 Maximum Efficiencies. The Carnot efficiency is the maximum thermodynamic efficiency that can be theoretically achieved by a power cycle consisting of reversible processes and operating between two thermal reservoirs at temperatures T_c and T_h. It is expressed as

$$\eta_{\mathrm{Carnot}} = 1 - \frac{T_c}{T_h} \tag{14}$$

Alternatively, the Curzon–Ahlborn efficiency η_{CA} represents the efficiency at the maximum power production of heat engines, which only considers the irreversibility of the finite rate heat transfer between thermal sources and working fluids (endoreversible engines) [58]. The Curzon–Ahlborn efficiency η_{CA} is expressed as [58]

$$\eta_{\mathrm{CA}} = 1 - \sqrt{\frac{T_c}{T_h}} \tag{15}$$

To assess the performance of the conceptual device, it is instructive to compare the efficiency of the device with both η_{Carnot} and η_{CA}.

4 Results and Discussion

4.1 Effect of Absorbing Layers. This section aims at assessing the effect of the SiO_2 absorbing layers on the device performance. The temperature oscillations of a PE plate consisting of a pyroelectric material 60/40 P(VDF-TrFE) film sandwiched between two aluminum electrodes were simulated with and without a 1.5 μm thick SiO_2 absorbing layers. The device was operated at $f=1$ Hz with the cold plate at $T_c=273$ K and the hot plate at $T_h=388$ K. Figure 3 shows the corresponding temperature variations of the PE plate as a function of time. It indicates that the PE plate with SiO_2 absorbing layers underwent a temperature swing of $\Delta T_{\mathrm{PE}}=63$ K, while that without absorbing layers reached 50 K. Therefore, the presence of SiO_2 absorbing layers enhanced the nanoscale radiative heat transfer from the cold and hot plates to the PE plate. This, in turn, increased the amplitude of the PE plate temperature oscillations. It also resulted in a higher operating frequency and a larger power density. Consequently, in view of these results, only the device with SiO_2 absorbing layers will be considered in the remaining part of the study.

4.2 Effect of Oscillation Frequency. As previously discussed, the energy density N_D is assumed to be a constant as long as the device is operated across the phase transition interval between temperatures T_{p1} and T_{p2}. Therefore, increasing the frequency of temperature oscillation in the PE plate will increase the power density of the device. On the other hand, the Olsen cycle using 60/40 P(VDF-TrFE) was experimentally performed across

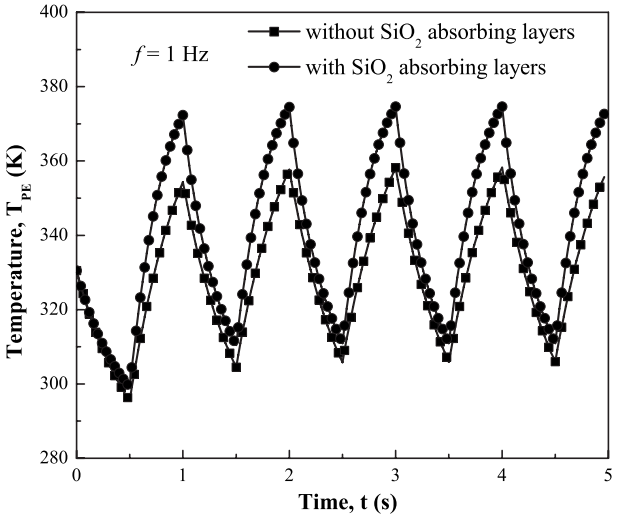

Fig. 3 Temperature oscillation of the PE plate made of 60/40 P(VDF-TrFE) as a function of time oscillating at 1 Hz between cold and hot plates at $T_c=273$ K and $T_h=388$ K, with and without SiO_2 absorbing layers

the phase transition occurring between temperatures $T_{p1}=313$ K and $T_{p2}=370$ K corresponding to $\Delta T_{\mathrm{PE}}=57$ K with $T_{\mathrm{Curie}}=348$ K and resulted in an energy density N_D of 279 J/l [17].

Figure 4(*a*) shows the PE temperature as a function of time at a frequency $f=0.6$ Hz for $T_c=273$ K and $T_h=388$ K. It indicates that the PE temperature oscillated between minimum and maximum temperatures $T_{\min}=297$ K and $T_{\max}=382$ K across the Curie temperature $T_{\mathrm{Curie}}=348$ K, ensuring a complete phase transition [17]. Similarly, Fig. 4(*b*) shows that the temperature oscillated between 315 K and 369 K at a frequency $f=1.2$ Hz. It is evident that the amplitude of the temperature oscillation decreased as the frequency increased. This result suggests that it is possible to achieve the desired temperature oscillation across the phase transition at a frequency ten times larger than that achieved by Olsen and co-workers using convective heat transfer [6].

In order to identify the largest frequency for which the temperature oscillation covers the phase transition, different frequencies were examined. Figure 5 shows the maximum and minimum temperatures reached by the PE plate made of 60/40 P(VDF-TrFE) with SiO_2 absorbing layers as a function of frequency. It indicates that for frequencies less than 1.2 Hz, the PE plate experienced temperature oscillations from below 313 K to above 370 K, thus covering the phase transition region [17]. According to Eq. (13), the maximum power output per unit surface area achieved was 0.84 mW/cm^2 at 1.2 Hz. This is more than twice the power output reported by Kouchachvili and Ikura [17].

Alternatively, by choosing a material exhibiting a very strong electrocaloric effect, the power density can be further increased. For example, the composite thin film 0.9PMN-PT features a volumetric heat capacity of $(\rho c_p)_{\mathrm{PE}}=3\times10^6$ J/m^3 K and an energy density of 432 J/l for a 10 K temperature variation from $T_{p1}=338$ K to $T_{p2}=348$ K [25,26]. Although such temperature interval is beyond the material Curie temperature of 333 K [26], it is still possible to generate a very large energy density due to the highly nonlinear behavior near that temperature. However, such composite films should be very thin in order to sustain very large electric fields and thus convert more heat into electric energy [25]. To achieve large power output per unit surface area with such a composite material, we considered a PE plate made of 100 layers of 300 nm 0.9PMN-PT thin films separated by 50 nm aluminum electrodes. The overall thicknesses of the pyroelectric material and aluminum electrodes were $L_{\mathrm{PE}}=30$ μm and $L_{\mathrm{Al}}=5$ μm, respectively. A 1.5 μm thick SiO_2 absorbing layer was also present

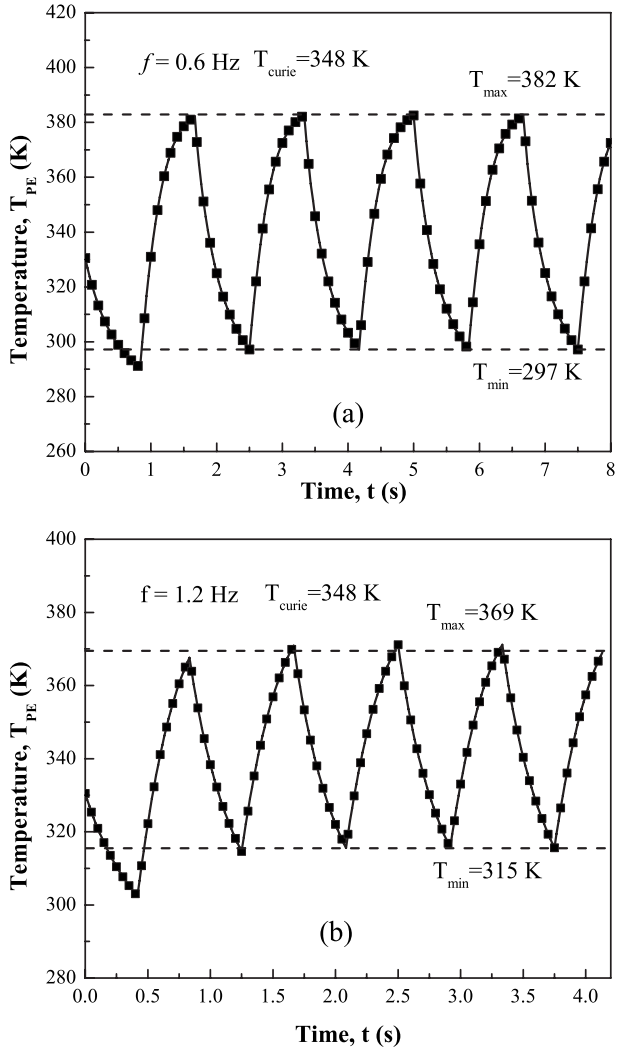

Fig. 4 Temperature oscillation of PE plate made of 60/40 P(VDF-TrFE) with SiO_2 absorbing layers as a function of time with T_c=273 K and T_h=388 K at frequencies of (*a*) *f*=0.6 Hz and (*b*) *f*=1.2 Hz

on both sides of the composite PE plate. Therefore, the overall PE plate thickness was L_t=38 μm, and the effective volumetric heat capacity was $(\rho c_p)_{\text{eff}}=2.82\times10^6$ J/m^3 K. The temperatures of the cold and hot plates were set as T_c=283 K and T_h=383 K, respectively, in order to achieve proper temperature oscillation. Figure 6 shows the maximum and minimum temperatures of oscillation as a function of frequency for the 0.9PMN-PT composite PE plate considered. Given the reported energy density N_D =432 J/l for 10 K temperature oscillations [25], the electrical power density $\dot{W}_e$ was estimated to be 6.5 mW/cm^2 at the working frequency of 5 Hz.

Finally, it is interesting to compare this power output with those of alternative technologies such as thermoelectric energy generators. A comparison was made between the PE device made of 60/40 P(VDF-TrFE) operating between $T_{\min}$=313 K and $T_{\max}$ =370 K at 1.2 Hz, and thermoelectric generators operated between 313 K and 370 K. For example, Böttner et al. [59] achieved a power density of 0.06 mW/cm^2 at a temperature difference of 5 K at around 300 K using *n*-Bi_2Te_3 and *p*-$(Bi,Sb)_2Te_3$ materials. Assuming that the efficiency of a thermoelectric generator increases nearly linearly with temperature difference [60], the thermoelectric generator may achieve 0.7 mW/cm^2 between 313 K and 370 K. Thus, it is comparable to the power density of

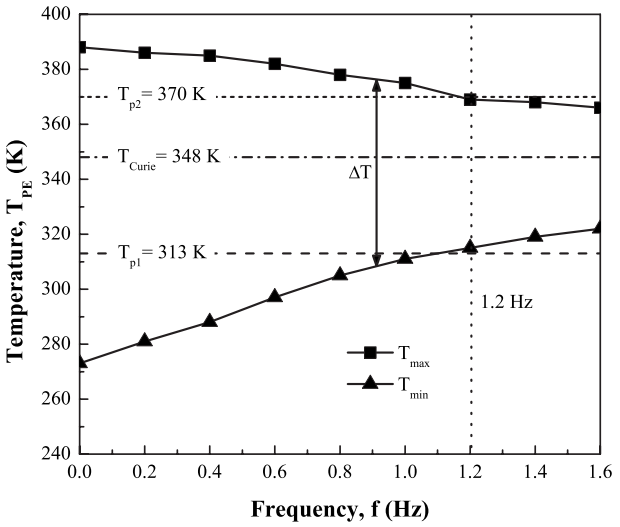

Fig. 5 Minimum and maximum temperatures of oscillation as a function of frequency for PE plate made of 60/40 P(VDF-TrFE) film with SiO_2 absorbing layers for T_c=273 K and T_h=388 K

0.84 mW/cm^2 obtained from the simulated results of the PE device using P(VDF-TrFE) for the same temperature difference.

4.3 Device Efficiency. To assess the device efficiency, the input power $\dot{W}_p$ consumed to oscillate the PE plate between the hot and cold sources was estimated. According to Eq. (12), the input oscillation power was estimated to be less than 10 μW/cm^2 for P(VDF-TrFE) at 1 Hz. This magnitude is also consistent with results reported in the literature for the piezoelectric material PZT [61]. Thus, the electrical power generated $\dot{W}_e$ was two orders of magnitude larger than the input power $\dot{W}_p$, which can thus be neglected. Similar results applied to the PE plate made of the 0.9PMN-PT thin film. Consequently, the maximum energy efficiency of the device η, defined by Eq. (10), could reach up to 0.2% at f=1.2 Hz for 60/40 P(VDF-TrFE). On the other hand, using the 0.9PMN-PT composite thin films resulted in an efficiency of 1.3% at f=5 Hz for a 10 K temperature difference. This is about 50 times larger than that estimated by van der Ziel [21].

Figure 7 shows the efficiency ratio $\eta/\eta_{\text{Carnot}}$ and η/η_{CA} as a

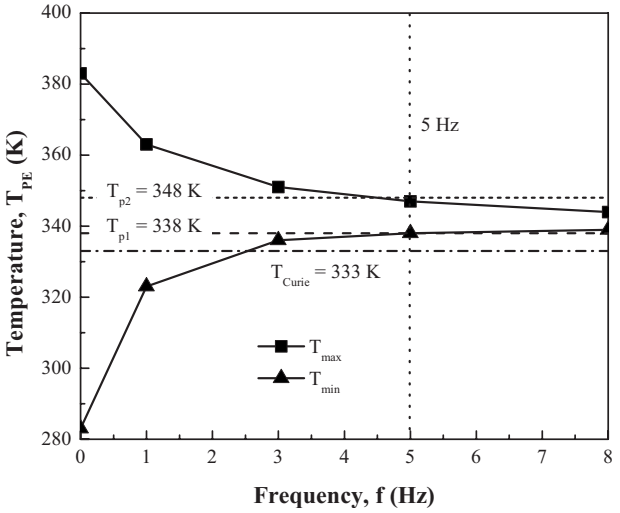

Fig. 6 Minimum and maximum temperatures of oscillation as a function of frequency for PE plate made of 0.9PMN-PT thin films with SiO_2 absorbing layers for T_c=283 K and T_h=383 K

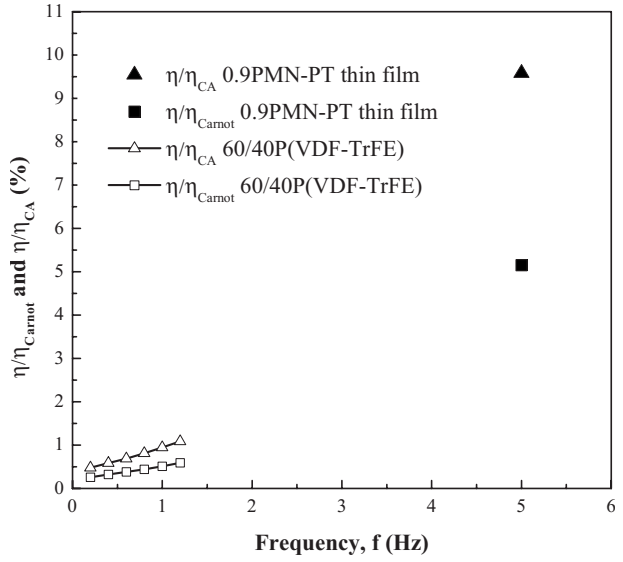

Fig. 7 Efficiency ratios η/η_{Carnot} and η/η_{CA} as a function of frequency for PE plates made (i) of 60/40 P(VDF-TrFE) for temperature oscillations shown in Fig. 5 and (ii) of 0.9PMN-PT ($T_{max}-T_{min}=10$ K) with SiO_2 absorbing layers

function of frequency for PE plates made of a single 60/40 P(VDF-TrFE) film and multiple films of 0.9PMN-PT with their electrodes. It suggests that by using the copolymer P(VDF-TrFE) at the operating frequency of 1.2 Hz with a 57 K temperature oscillation amplitude, up to 0.6% of the Carnot efficiency or 1.2% of the Curzon–Ahlborn efficiency can be achieved between $T_c=273$ K and $T_h=388$ K. As a reference, it is worth mentioning that Olsen and Bruno [6] experimentally obtained efficiencies that were about one magnitude smaller than the numerical results above using 73/27 P(VDF-TrFE) for the Olsen cycle between 296 K and 340 K. As for the 0.9PMN-PT composite plate, the efficiency at the operating frequency of 5 Hz for a 10 K temperature oscillation amplitude corresponds to 5% of the Carnot efficiency and 10% of the Curzon–Ahlborn efficiency for temperatures $T_c=283$ K and $T_h=383$ K.

4.4 Discussion. The 0.9PMN-PT composite thin film may feature an even larger energy density if the device was operated across the whole phase transition temperature interval, taking advantage of the nonlinear effect around the Curie temperature. Then, the device would reach a larger power output and higher efficiency. Alternatively, synthesis and processing of pyroelectric/ferroelectric materials with a larger energy density N_D should be explored. In addition, a multistage pyroelectric plate consisting of superimposed pyroelectric films with different Curie temperatures could be envisioned to harvest more energy through a wider phase transition region and to further increase the output energy density and efficiency of the device. A prototype of such a device should be experimentally assembled and operated to establish the feasibility of the concept investigated in this manuscript. Finally, a life cycle analysis of the device should also be performed to fully assess its usefulness.

Finally, note that (i) parallelism is not essential to the device operation and (ii) a gap smaller than 100 nm, if it can be achieved in practice, would result in larger temperature oscillations or operating frequencies for a given temperature swing. In turn, the power density and efficiency of the device would increase. Touching, however, would not be beneficial since heat transfer would then be by conduction, which is slow and limited by the thermal contact resistance between the PE plate and the cold or hot plates.

5 Conclusion

This paper combines, for the first time, nanoscale thermal radiation and pyroelectric energy conversion for harvesting low grade waste heat. The nanoscale radiation model was validated against results reported in the literature. The proposed device made use of the enhanced radiative heat transfer across a nanosize gap to achieve high operating frequencies or large temperature oscillations in a composite PE plate. The hot and cold plates were coated with a SiO_2 absorbing layer to further enhance the radiative heat fluxes. The maximum efficiency and power density for a PE plate made of 60/40 P(VDF-TrFE) operated between 273 K and 388 K were found to be 0.2% and 0.84 mW/cm^2, respectively. The PE plate made of the 0.9PMN-PT composite thin films achieved a higher efficiency and a larger power output, namely, 1.3% and 6.5 mW/cm^2, respectively, for a temperature oscillation amplitude of 10 K around 343 K at 5 Hz.

Nomenclature

c = speed of light in vacuum ($c=2.998\times10^8$ m/s)
c_p = specific heat (J/kg K)
d = distance between two parallel plates (μm)
$d_{PE,c}$, $d_{PE,h}$ = distance between the PE plate and the cold and hot plates, respectively (μm)
f = cycle frequency (Hz)
$\hbar$ = reduced Planck's constant ($\hbar=1.055\times10^{-34}$ J s)
h_r = radiative heat transfer coefficient (W/m^2 K)
H = Hamaker constant (J)
i = electrical current (A)
$I^0_{b\omega}$ = spectral blackbody radiation intensity (W/m^2)
k = thermal conductivity (W/m K)
k_B = Boltzmann's constant ($k_B=1.3806\times10^{-23}$ J/K)
L = film thickness (μm)
L_t = total PE plate thickness (μm)
N_q = numbers of wavevectors
N_ω = numbers of frequencies
N_D = energy density of pyroelectric material (J/l)
p = z-component of wavevector (rad/m)
p_c = pyroelectric coefficient (μC/m^2 K)
P_c = Casimir pressure (Pa)
P_g = gravitational pressure (Pa)
P_{rad} = radiation pressure (Pa)
P_v = van der Waals pressure (Pa)
q = x-component of wavevector (rad/m)
q'' = heat flux (W/m^2)
$\dot{Q}_{in}$ = average net heat flux from the hot plate to the PE plate (W/m^2)
r = Fresnel coefficient
s_1 = z-component of the wavevector in medium 1 ($s_1=\sqrt{\varepsilon_{r1}\omega^2/c^2-q^2}$)
t = time (s)
T = temperature (K)
T_{Curie} = Curie temperature (K)
$\dot{W}_e$ = average generated electrical power (mW/cm^2)
$\dot{W}_p$ = average input oscillation power (mW/cm^2)
x,z = transverse and longitudinal coordinates

Greek Symbols

$\alpha_{1,2}$ = total hemispherical emissivity
ε_0 = dielectric permittivity of vacuum ($\varepsilon_0=8.85\times10^{-12}$ F/m)
ε_r = dielectric constant

$\Phi_{12}(\omega,d)$ = spectral efficiency in radiation transfer between media 1 and 2
γ = relaxation frequency (rad/s)
η_{Carnot}, η_{CA} = Carnot and Curzon–Ahlborn efficiencies
λ = wavelength (μm)
ρ = density (kg/m^3)
σ = Stefan–Boltzmann constant ($\sigma=5.67\times10^{-8}$ W/m^2 K^4)
τ = cycle period ($\tau=1/f$) (s)
ω = angular frequency (rad/s)
ω_0 = oscillator frequency (rad/s)
ω_p = plasma frequency (rad/s)

Subscripts

1, 2, 3 = refers to media 1, 2, and 3
Al = Al electrodes
b = blackbody
c = cold plate
eff = effective properties of the PE plate
h = hot plate
p = phase transition
PE = PE thin film or plate
ω = refers to values at frequency ω

References

[1] Lawrence Livermore National Laboratory, 2008, "U.S. Energy Flow Trends—2002," https://eed.llnl.gov/flow/02flow.php
[2] Olsen, R., 1982, "Ferroelectric Conversion of Heat to Electrical Energy—A Demonstration," J. Energy, **6**(2), pp. 91–95.
[3] Olsen, R., Bruno, D., and Briscoe, J., 1984, "Cascaded Pyroelectric Energy Converter," Ferroelectrics, **59**(1), pp. 205–219.
[4] Olsen, R., Bruno, D., Briscoe, J., and Butler, W., 1981, "A Pyroelectric Energy Converter Which Employs Regeneration," Ferroelectrics, **38**(1–4), pp. 975–978.
[5] Olsen, R., and Brown, D., 1982, "High-Efficiency Direct Conversion of Heat to Electrical Energy-Related Pyroelectric Measurements," Ferroelectrics, **40**(1–2), pp. 17–27.
[6] Olsen, R., Bruno, D., and Briscoe, J. M., 1985, "Pyroelectric Conversion Cycle of Vinylidene Fluoride-Trifluoroethylene Copolymer," J. Appl. Phys., **57**(11), pp. 5036–5042.
[7] Olsen, R., Bruno, D., and Briscoe, J. M., 1985, "Pyroelectric Conversion Cycles," J. Appl. Phys., **58**(12), pp. 4709–4716.
[8] Ikura, M., 2002, "Conversion of Low-Grade Heat to Electricity Using Pyroelectric Copolymer," Ferroelectrics, **267**(6), pp. 403–408.
[9] Kouchachvili, L., and Ikura, M., 2007, "Pyroelectric Conversion-Effects of P(VDF-TrFE) Preconditioning on Power Conversion," J. Electrost., **65**(3), pp. 182–188.
[10] Olsen, R., and Bruno, D., 1986, "Pyroelectric Conversion Materials," *Proceedings of the 21st Intersociety Energy Conversion Engineering Conference*, pp. 89–93.
[11] Vanderpool, D., Yoon, J., and Pilon, L., 2008, "Simulations of a Prototypical Device Using Pyroelectric Materials for Harvesting Waste Heat," Int. J. Heat Mass Transfer, **51**, pp. 5052–5062.
[12] Nguyen, H. T., Navid, A., and Pilon, L., 2010, "Improved Pyroelectric Energy Converter for Waste Heat Energy Harvesting Using Co-Polymer P(VDF-TrFE) and Olsen Cycle," Appl. Therm. Eng., to be published.
[13] Lang, S. B., 2005, "Pyroelectricity: From Ancient Curiosity to Modern Imaging Tool," Phys. Today, **58**(8), pp. 31–36.
[14] Cravalho, E. G., Tien, C. L., and Caren, R. P., 1967, "Effect of Small Spacings on Radiative Transfer Between Two Dielectrics," ASME J. Heat Transfer, **89**(4), pp. 351–358.
[15] Polder, D., and Van Hove, M., 1971, "Theory of Radiative Heat Transfer Between Closely Spaced Bodies," Phys. Rev. B, **4**(10), pp. 3303–3314.
[16] Olsen, R., and Evans, D., 1983, "Pyroelectric Energy Conversion—Hysteresis Loss and Temperature Sensitivity of a Ferroelectric Material," J. Appl. Phys., **54**(10), pp. 5941–5944.
[17] Kouchachvili, L., and Ikura, M., 2008, "Improving the Efficiency of Pyroelectric Conversion," Int. J. Energy Res., **32**(4), pp. 328–335.
[18] Navid, A., Lynch, C. S., and Pilon, L., 2010, "Purified and Porous Poly(Vinylidene Fluoride-Trifluoroethylene) Thin Films for Pyroelectric Infrared Sensing and Energy Harvesting," Smart Mater. Struct., **19**, p. 055006.
[19] Clingman, W. H., and Moore, R. G., 1961, "Application of Ferroelectricity to Energy Conversion Processes," J. Appl. Phys., **32**(4), pp. 675–681.
[20] Fatuzzo, E., Kiess, H., and Nitsche, R., 1966, "Theoretical Efficiency of Pyroelectric Power Converters," J. Appl. Phys., **37**(2), pp. 510–516.
[21] van der Ziel, A., 1974, "Solar Power Generation With the Pyroelectric Effect," J. Appl. Phys., **45**(9), p. 4128.
[22] Itskovsky, M. A., 1999, "Pyroelectric Hysteresis Loop at Ferroelectric Phase Transition," J. Appl. Phys., **85**(8), pp. 4256–4258.
[23] Smolenskii, G. A., Krainik, N. N., Khuchua, N. P., Zhdanova, V. V., and Mylnikova, I. E., 1966, "The Curie Temperature of $LiNbO_3$," Phys. Status Solidi B, **13**(2), pp. 309–314.
[24] Gonzalo, J. A., 1976, "Ferroelectric Materials as Energy Converters," Ferroelectrics, **11**(1), pp. 423–430.
[25] Sebald, G., Pruvost, S., and Guyomar, D., 2008, "Energy Harvesting Based on Ericsson Pyroelectric Cycles in a Relaxor Ferroelectric Ceramic," Smart Mater. Struct., **17**(1), p. 015012.
[26] Mischenko, A. S., Zhang, Q., Whatmore, R. W., Scott, J. F., and Mathur, N. D., 2006, "Giant Electrocaloric Effect in the Thin Film Relaxor Ferroelectric $0.9PbMg_{1/3}Nb_{2/3}O_3-0.1PbTiO_3$ Near Room Temperature," Appl. Phys. Lett., **89**(24), p. 242912.
[27] Rytov, S. M., 1953, *Theory of Electrical Fluctuation and Thermal Radiation*, Academy of Science of USSR, Moscow.
[28] Mulet, J. P., Joulain, K., Carminati, R., and Greffet, J. J., 2002, "Enhanced Radiative Heat Transfer at Nanometric Distances," Microscale Thermophys. Eng., **6**(3), pp. 209–222.
[29] DiMatteo, R. S., Greiff, P., Finberg, S. L., Young-Waithe, K. A., Choy, H. K. H., Masaki, M. M., and Fonstad, C. G., 2001, "Enhanced Photogeneration of Carriers in a Semiconductor Via Coupling Across a Nonisothermal Nanoscale Vacuum Gap," Appl. Phys. Lett., **79**(12), pp. 1894–1896.
[30] Whale, M. D., and Cravalho, E. G., 2002, "Modeling and Performance of Microscale Thermophotovoltaic Energy Conversion Devices," IEEE Trans. Energy Convers., **17**(1), pp. 130–142.
[31] Zhang, Z. M., Fu, C. J., and Zhu, Q. Z., 2003, "Optical and Thermal Radiative Properties of Semiconductors Related to Micro/Nanotechnology," Adv. Heat Transfer, **37**, pp. 179–296.
[32] Hargreaves, C., 1969, "Anomalous Radiative Transfer Between Closely-Spaced Bodies," Phys. Lett., **30A**(9), pp. 491–492.
[33] Domoto, G. A., Boehm, R. F., and Tien, C. L., 1970, "Experimental Investigation of Radiative Transfer Between Metallic Surfaces at Cryogenic Temperatures," ASME J. Heat Transfer, **92**(3), pp. 412–417.
[34] Kittel, A., Wischnath, U. F., Welker, J., Huth, O., Ruting, F., and Biehs, S. A., 2008, "Near-Field Thermal Imaging of Nanostructured Surfaces," Appl. Phys. Lett., **93**(19), p. 193109.
[35] Pan, J. L., 2000, "Radiative Transfer Over Small Distances From a Heated Metal," Opt. Lett., **25**(6), pp. 369–371.
[36] Pan, J. L., Choy, H. K. H., and Fonstad, C. G., 2000, "Very Large Radiative Transfer Over Small Distances From a Blackbody for Thermophotovoltaic Applications," IEEE Trans. Electron Devices, **47**(1), pp. 241–249.
[37] Loomis, J., and Maris, H., 1994, "Theory of Heat Transfer by Evanescent Electromagnetic-Waves," Phys. Rev. B, **50**(24), pp. 18517–18524.
[38] Pendry, J. B., 1999, "Radiative Exchange of Heat Between Nanostructures," J. Phys.: Condens. Matter, **11**(35), pp. 6621–6633.
[39] Hu, L., Narayanaswamy, A., Chen, X., and Chen, G., 2008, "Near-Field Thermal Radiation Between Two Closely Spaced Glass Plates Exceeding Planck's Blackbody Radiation Law," Appl. Phys. Lett., **92**(13), p. 133106.
[40] Narayanaswamy, A., Shen, S., and Chen, G., 2008, "Near-Field Radiative Heat Transfer Between a Sphere and a Substrate," Phys. Rev. B, **78**(11), p. 115303.
[41] Narayanaswamy, A., Shen, S., Hu, L., Chen, X. Y., and Chen, G., 2009, "Breakdown of the Planck Blackbody Radiation Law at Nanoscale Gaps," Appl. Phys. A: Mater. Sci. Process., **96**(2), pp. 357–362.
[42] Shen, S., Narayanaswamy, A., and Chen, G., 2009, "Surface Phonon Polaritons Mediated Energy Transfer Between Nanoscale Gaps," Nano Lett., **9**(8), pp. 2909–2913.
[43] Biehs, S. A., Reddig, D., and Holthaus, M., 2007, "Thermal Radiation and Near-Field Energy Density of Thin Metallic Films," Eur. Phys. J. B, **55**(3), pp. 237–251.
[44] Biehs, S. A., 2007, "Thermal Heat Radiation, Near-Field Energy Density and Near-Field Radiative Heat Transfer of Coated Materials," Eur. Phys. J. B, **58**(4), pp. 423–431.
[45] Francoeur, M., Mengüç, M. P., and Vaillon, R., 2008, "Near-Field Radiative Heat Transfer Enhancement Via Surface Phonon Polaritons Coupling in Thin Films," Appl. Phys. Lett., **93**(4), p. 043109.
[46] Fu, C. J., and Tan, W. C., 2009, "Near-Field Radiative Heat Transfer Between Two Plane Surfaces With One Having a Dielectric Coating," J. Quant. Spectrosc. Radiat. Transf., **110**(12), pp. 1027–1036.
[47] Volokitin, A. I., and Persson, B. N. J., 2001, "Radiative Heat Transfer Between Nanostructures," Phys. Rev. B, **63**(20), p. 205404.
[48] Modest, M., 2003, *Radiative Heat Transfer*, Academic, San Diego, CA.
[49] Joulain, K., Mulet, J. P., Marquier, F., Carminati, R., and Greffet, J. J., 2005, "Surface Electromagnetic Waves Thermally Excited: Radiative Heat Transfer, Coherence Properties and Casimir Forces Revisited in the Near Field," Surf. Sci. Rep., **57**(3–4), pp. 59–112.
[50] Brewster, M. Q., 1992, *Thermal Radiative Transfer and Properties*, Wiley-Interscience, New York.
[51] Chan, H. B., Aksyuk, V. A., Kleiman, R. N., Bishop, D. J., and Capasso, F., 2001, "Quantum Mechanical Actuation of Microelectromechanical Systems by the Casimir Force," Science, **291**(5510), pp. 1941–1944.
[52] Bohren, C. F., and Huffman, D. R., 2004, *Absorption and Scattering of Light by Small Particles*, Wiley-Interscience, New York.
[53] Casimir, H. B. G., and Polder, D., 1948, "The Influence of Retardation on the London-van der Waals Forces," Phys. Rev., **73**(4), pp. 360–372.
[54] Serry, F. M., Walliser, D., and Maclay, G. J., 1995, "The Anharmonic Casimir Oscillator (ACO)—The Casimir Effect in a Model Microelectromechanical System," J. Microelectromech. Syst., **4**(4), pp. 193–205.

[55] Mostepanenko, V. M., and Trunov, N. N., 1997, *The Casimir Effect and Its Applications*, Oxford University Press, New York.
[56] Israelachvili, J., 1992, *Intermolecular and Surface Forces*, Academic, San Diego, CA.
[57] Nichols, E. F., and Hull, G. F., 1903, "The Pressure Due to Radiation," Astrophys. J., **17**(1), pp. 315–351.
[58] Curzon, F. L., and Ahlborn, B., 1975, "Efficiency of a Carnot Engine at Maximum Power Output," Am. J. Phys., **43**(1), pp. 22–24.
[59] Böttner, H., Nurnus, J., Gavrikov, A., Kühner, G., Jägle, M., Künzel, C., Eberhard, D., Plescher, G., Schubert, A., and Schlereth, K. H., 2004, "New Thermoelectric Components Using Microsystem Technologies," J. Microelectromech. Syst., **13**(3), pp. 414–420.
[60] Priya, S., and Inman, D. J., 2009, *Energy Harvesting Technologies*, Springer, New York.
[61] Jordan, T., Ounaies, Z., Tripp, J., and Tcheng, P., 1999, "Electrical Properties and Power Considerations of a Piezoelectric Actuator," Mater. Res. Soc. Symp. Proc., **604**, pp. 203–208.